Factors Influencing the Site of Electroreduction in Rhodium Porphyrins

K. M. Kadish,*[1a] Y. Hu,[1a] T. Boschi,[1b] and P. Tagliatesta*[1a,b]

Department of Chemistry, University of Houston, Houston, Texas 77204-5641, and Dipartimento di Scienze e Tecnologie Chimiche, II Università degli Studi di Roma, Via O. Raimondo, 00173 Roma, Italy

Received December 17, 1992

The electrochemistry of rhodium(III) porphyrins containing bound phosphine, isocyanide, or carbene axial ligands was investigated by cyclic voltammetry and UV–visible spectroelectrochemistry in tetrahydrofuran (THF) and methylene chloride (CH_2Cl_2) containing tetrabutylammonium hexafluorophosphate ($TBAPF_6$) as supporting electrolyte. The investigated compounds are represented as $[(TPP)Rh(L)_2]PF_6$, $(TPP)Rh(L')PF_6$, or $(TPP)Rh(PF_3)(OH)$, where TPP is the dianion of tetraphenylporphyrin, L = PPh_3, PPh_2Me, $PPhMe_2$, and $CNCH_2Ph$, and L' = $:C(NHCH_2Ph)_2$. The addition of one electron to these complexes leads to one of two different reduction products depending upon the temperature and the specific set of axial ligands. Some of the complexes are reversibly reduced by one electron to give a transient Rh(III) porphyrin π anion radical while others are irreversibly reduced under the same solution conditions to give dimeric $[(TPP)Rh]_2$. In several cases, the addition of one electron gives a Rh(II) dimer at room temperature but a Rh(III) π anion radical at low temperature. The UV–visible data suggest that all of the investigated rhodium(III) porphyrins are initially reduced at the porphyrin π ring system, and this is also the conclusion based on electrochemical criteria relating the potentials for oxidation and reduction of each metalloporphyrin in nonaqueous media. The absolute potential difference between $E_{1/2}$ for the first room temperature oxidation of a given complex in CH_2Cl_2 and the first low-temperature reduction of the same species in THF (where the reaction is reversible) ranges between 2.22 and 2.32 V, suggesting that both electrode reactions involve the porphyrin π ring system. One of the species, $(TPP)Rh(PF_3)(OH)$, undergoes a slow conversion of the electrogenerated π anion radical to dimeric $[(TPP)Rh]_2$, and this reaction was followed as a function of time by thin-layer UV–visible spectroelectrochemistry in THF. Exchange equilibria involving bound PPh_3 and THF axial ligands were also studied in methylene chloride or tetrahydrofuran by UV–visible spectroscopy. Both $[(TPP)Rh(PPh_3)]^+$ and $[(TPP)Rh(PPh_3)_2]^+$ are converted to $[(TPP)Rh(PPh_3)(THF)]^+$ in neat THF, but the addition of 1.0 equiv of PPh_3 to these solutions leads to $[(TPP)Rh(PPh_3)_2]^+$ as identified by UV–visible spectroscopy. The formation constant for this reaction was calculated as $10^{3.1}$ using spectrophotometric methods.

Introduction

A variety of rhodium tetraphenylporphyrins with halogen, nitrogen, phosphorus, or carbon σ-bonded axial ligands have been electrochemically characterized.[2-11] The oxidation of these compounds invariably occurs at the conjugated macrocycle to give π cation radicals and dications,[3,5,7,9] while the reduction can occur at one of several sites on the complex and may or may not be followed by dimerization to give $[(TPP)Rh]_2$, where TPP is the dianion of tetraphenylporphyrin. It is known that an electron may be added to the metal center,[4-6,8] to the porphyrin π ring system,[9] or, in some cases, to the fifth or sixth axial ligand[10] of a given monomeric Rh(III) porphyrin, but the exact factors associated with the initial site of reduction as well as with the stability of the final reduction product are not totally understood. Some electrogenerated complexes are relatively stable on the spectroelectrochemical time scale, but this is not the case for others which rapidly dimerize to give $[(P)Rh]_2$ as a final porphyrin product.[2]

The lack of rapid dimerization for some singly reduced rhodium porphyrin complexes might be accounted for by steric and/or electronic effects of the axial ligand but may also be related to the site of electron transfer, i.e., to formation of a Rh(III) π anion radical rather than a Rh(III) porphyrin species. This is investigated in the present paper which reports the electrochemistry and spectroelectrochemistry of Rh(III) porphyrins with bound carbene, phosphine, or isocyanide axial ligands. The investigated compounds are represented as $[(TPP)Rh(L)_2]PF_6$, $(TPP)Rh(L')PF_6$, and $(TPP)Rh(PF_3)(OH)$, where TPP is the dianion of tetraphenylporphyrin and L = PPh_3, PPh_2Me, $PPhMe_2$, or $CNCH_2Ph$ and L' = $:C(NHCH_2Ph)_2$. As will be shown, all of the porphyrins undergo an initial one-electron addition to the porphyrin π ring system, and none show evidence for an expected Rh(III)/Rh(II) process. This is quite unexpected and has never before been demonstrated.

Experimental Section

Chemicals. Spectroanalyzed-grade methylene chloride (CH_2Cl_2), from Fisher Chemical Co., was distilled under nitrogen, first over P_2O_5 and then over CaH_2. Commercial-grade tetrahydrofuran (THF) from Aldrich Chemical Co. was distilled from $LiAlH_4$ under nitrogen. Tetra-*n*-butylammonium hexafluorophosphate ($TBAPF_6$) was purchased from Fluka Chemical Co., twice recrystallized from absolute ethyl alcohol, and then stored in a vacuum oven at 40 °C. Phosphorus trifluoride (PF_3) was purchased from Rivoira-Spa, Italy, and was provided by Union Carbide, Westerlo, Belgium, in 99.9% purity.

$[(TPP)Rh(PPh_3)_2]PF_6$, $[(TPP)Rh(PPh_2Me)_2]PF_6$, $[(TPP)Rh(PPhMe_2)_2]PF_6$, $(TPP)Rh{=}C(NHCH_2Ph)_2PF_6$, and $[(TPP)Rh(CNCH_2Ph)_2]PF_6$ were prepared as described in the literature,[12,13] and their purity

(1) (a) University of Houston and (b) II Università Degli Studi di Roma.
(2) Guilard, R.; Kadish, K. M. *Chem. Rev.* **1988**, *88*, 1121.
(3) Wayland, B. B.; Newman, A. R. *Inorg. Chem.* **1981**, *20*, 3093.
(4) Anderson, J. E.; Yao, C.-L.; Kadish, K. M. *Inorg. Chem.* **1986**, *25*, 3224.
(5) Kadish, K. M.; Yao, C.-L.; Anderson, J. E.; Cocolios, P. *Inorg. Chem.* **1985**, *24*, 4515.
(6) Anderson, J. E.; Yao, C.-L.; Kadish, K. M. *J. Am. Chem. Soc.* **1987**, *109*, 1106.
(7) Kadish, K. M.; Anderson, J. E.; Yao, C.-L.; Guilard, R. *Inorg. Chem.* **1986**, *25*, 1277.
(8) Anderson, J. E.; Yao, C.-L.; Kadish, K. M. *Inorg. Chem.* **1986**, *25*, 718.
(9) Kadish, K. M.; Araullo, C.; Yao, C.-L. *Organometallics* **1988**, *7*, 1583.
(10) Anderson, J. E.; Liu, Y. H.; Kadish, K. M. *Inorg. Chem.* **1987**, *26*, 4174.
(11) Thackray, D. C.; Ariel, D.; Leung, T. W.; Menon, K.; James, B. R.; Trotter, J. *Can. J. Chem.* **1986**, *64*, 2440.
(12) Boschi, T.; Licoccia, S.; Tagliatesta, P. *Inorg. Chim. Acta* **1987**, *126*, 157.

0020-1669/93/1332-2996$04.00/0

was checked by mass spectrometry and ^{1}H NMR. These compounds are represented in the text of the discussion as $[(P)Rh(PPh_3)_2]^+$, $[(P)Rh(PPh_2Me)_2]^+$, $[(P)Rh(PPhMe_2)_2]^+$, $[(P)Rh{=}C(NHCH_2Ph)_2]^+$, and $[(P)Rh(CNCH_2Ph)_2]^+$.

(TPP)Rh(PPh$_3$)PF$_6$. A 375-mg amount of (TPP)RhCl (0.5 mmol) and 253 mg (1 mmol) of $AgPF_6$ were dissolved in 20 mL of dry acetone and stirred at room temperature under nitrogen for 30 min, after which 145 mg (0.55 mmol) of PPh_3 was added to solution and the stirring continued for another 2 h. The solvent was then evaporated and the residue chromatographed on silica gel, eluting with $CHCl_3$. The final product was recrystallized three times from $CHCl_3$/diethyl ether and gave a final yield of 85%. Anal. Calcd for $C_{62}H_{43}N_4F_6RhP_2$: C, 66.32; H, 3.86; N, 4.99. Found: C, 66.45; H, 3.73; N, 5.15. ^{1}H NMR ($CDCl_3$) δ 3.88 (t, 6 H, *o*-phenyl phos), 6.64 (t, 6 H, *m*-phenyl phos), 7.06 (t, 3 H, *p*-phenyl phos), 7.76 (m, 16 H, *o,m*-phenyl porp), 8.12 (m, 4 H, *p*-phenyl porp), 8.85 (s, 8 H, pyr); MS *m/e* 977 (M^+, 75), 715 ($M^+ - PPh_3$, 100).

(TPP)Rh(PF$_3$)(OH). A 200-mg amount of (TPP)RhCl (0.26 mmol) was dissolved in 100 mL of dry and argon-degassed methylene chloride. The solution was cooled to −80 °C, after which PF_3 gas was bubbled through the solution for 1 min at atmospheric pressure. The temperature was then allowed to rise and kept at 20 °C for 4 h. Argon was passed through the solution for 10 min, and after evaporation of the solvent, the final product was twice recrystallized from CH_2Cl_2/methanol to give a yield of 80%. Anal. Calcd for $C_{44}H_{29}N_4F_3PORh$: C, 64.40; H, 3.56; N, 6.83. Found: C, 64.33; H, 3.67; N, 6.84. ^{1}H NMR ($CDCl_3$) δ 7.96 (m, 16 H, *o,m*-phenyl porp), 8.27 (m, 4 H, *p*-phenyl porp), 8.94 (s, 8 H, pyr); MS *m/z* 802 ($M^+ - H$, 100), 715 ($M^+ - PF_3$, 94).

Instrumentation and Procedure. Cyclic voltammetric measurements were performed with a three-electrode system using an EG&G Princeton Applied Research Model 174A polarographic analyzer coupled with an EG&G Model 9002A X–Y recorder. The working electrode was a platinum button with a surface area of 0.8 mm^2. A large surface area platinum wire served as the auxiliary electrode. A homemade aqueous saturated calomel electrode (SCE) was used as the reference electrode and was separated from the bulk of the solution by a salt bridge filled with the solvent/supporting electrolyte mixture.

UV–visible spectra of the unreduced complexes were taken with an IBM Model 9430 UV–visible spectrophotometer while those of the neutral and singly reduced porphyrins were monitored with a Tracor Northern TN-6500 rapid-scan spectrophotometer. NMR spectra were obtained with a General Electric QE-300 NMR spectrometer. Mass spectra were taken on a VG-70 SEZ mass spectrometer.

Solutions for spectroelectrochemical measurements contained 0.2 M tetra-*n*-butylammonium hexafluorophosphate ($TBAPF_6$) as supporting electrolyte while those for cyclic voltammetry contained 0.1 M $TBAPF_6$. Deaeration was performed with solvent-saturated nitrogen or argon, and a positive pressure of the inert gas was maintained above the solution while making the measurements.

The design of the thin-layer spectroelectrochemical cell is described in the literature.[14] Routine low-temperature cyclic voltammograms were performed with the electrochemical cell inserted into an acetone/dry ice bath while low-temperature UV–visible spectroelectrochemistry was carried out by installing the spectroelectrochemical cell inside a specially designed Dewar which had a quartz optical window. Cooling of the solution was carried out by precooled nitrogen which was introduced into the Dewar containing the cell. The temperature in the cell under these conditions was monitored by an Omega Model 600 digital temperature meter.

Results and Discussion

Spectral Characterization of Triphenylphosphine Derivatives. The UV–visible spectrum of $[(P)Rh(PPh_3)]^+$ and $[(P)Rh(PPh_3)_2]^+$ in CH_2Cl_2 are shown in Figures 1a and 1c, respectively. The mono-PPh_3 complex is characterized by a Soret band at 414 nm and a single Q band at 525 nm while the bis-PPh_3 derivative, $[(P)Rh(PPh_3)_2]^+$, has a Soret band at 448 nm and two Q bands at 557 and 597 nm.

The addition of 1 equiv of PPh_3 to $[(P)Rh(PPh_3)]^+$ in CH_2Cl_2 gives a spectrum characteristic of $[(P)Rh(PPh_3)_2]^+$, and this UV–visible spectrum does not change upon continued addition of PPh_3. The spectrum of $[(P)Rh(PPh_3)_2]^+$ in CH_2Cl_2 is similar to the spectra of $(P)Rh(CH_3)(PPh_3)$ (λ = 439, 549, 590 nm)[9] and $[(P)Rh(O_2)(PPh_3)]^+$ (λ = 437, 546, 584 nm)[4] and also agrees with a spectrum obtained after addition of excess PPh_3 to solutions of $[(P)Rh(O_2)(PPh_3)]^+$ in CH_2Cl_2.[4]

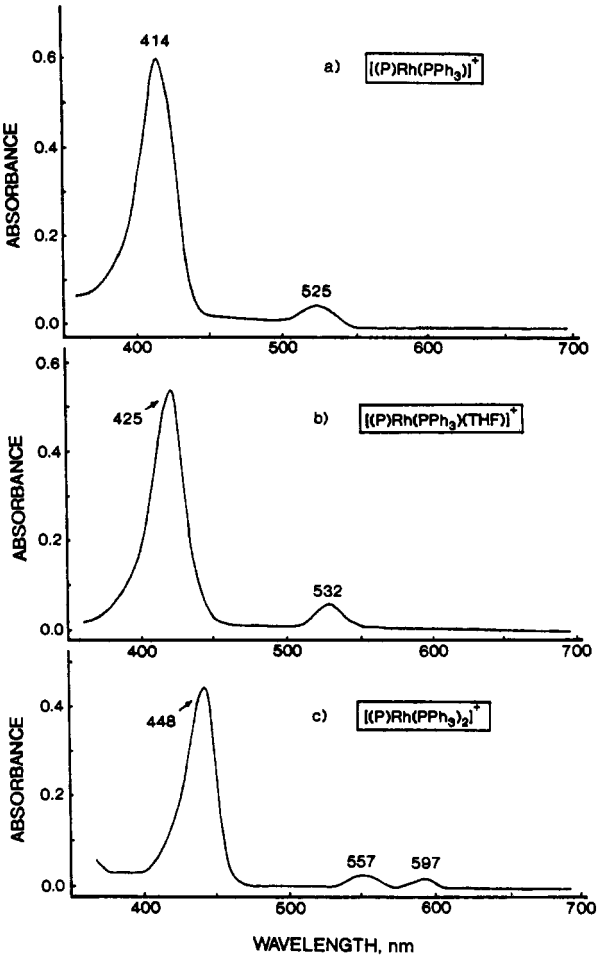

Figure 1. UV–visible spectra of (a) $[(P)Rh(PPh_3)]^+$, (b) $[(P)Rh(PPh_3)(THF)]^+$, and (c) $[(P)Rh(PPh_3)_2]^+$ in CH_2Cl_2.

$[(P)Rh(PPh_3)]^+$ can be converted to $[(P)Rh(PPh_3)(THF)]^+$ in CH_2Cl_2 by addition of 1.0 equiv of THF to solution, and this latter spectrum is shown in Figure 1b. The mixed-ligated species has bands at 425 and 532 nm and can also be generated from the bis-PPh_3 complex, $[(P)Rh(PPh_3)_2]^+$, in CH_2Cl_2/THF mixtures containing >1 M THF. Both the mono- and bis-phosphine complexes are converted to $[(P)Rh(PPh_3)(THF)]^+$ in neat THF at room temperature, but $[(P)Rh(PPh_3)_2]^+$ is spectroscopically detected in THF containing excess PPh_3. The resulting UV–visible data for formation of this species upon addition of PPh_3 to $[(P)Rh(PPh_3)(THF)]^+$ in THF are shown in Figure 2a. Diagnostic plots of $\log[(A - A_i)/(A_f - A)]$ vs $\log[PPh_3]$ were constructed using the absorbances at 425 and 448 nm and give a slope of 1.04 (see Figure 2b), which indicates the binding of only a single PPh_3 ligand as shown in the equation:

$$[(P)Rh(PPh_3)(THF)]^+ + PPh_3 \rightleftarrows [(P)Rh(PPh_3)_2]^+ + THF \quad (1)$$

The equilibrium constant for the above reaction is 1.3×10^3 and was calculated from the data in Figure 2. This value is slightly smaller than the 3.9×10^3 obtained for the binding of PPh_3 to $(TPP)Rh(CH_3)$ in CH_2Cl_2[9] but larger than the formation constant of 1.1×10^2 for the replacement of O_2 by PPh_3 on $(TPP)Rh(O_2)(PPh_3)$ in CH_2Cl_2.[4]

(13) Boschi, T.; Licoccia, S.; Paolesse, R.; Tagliatesta, P. *Organometallics* **1989**, *8*, 330.
(14) Lin, X. Q.; Kadish, K. M. *Anal. Chem.* **1985**, *57*, 1498.

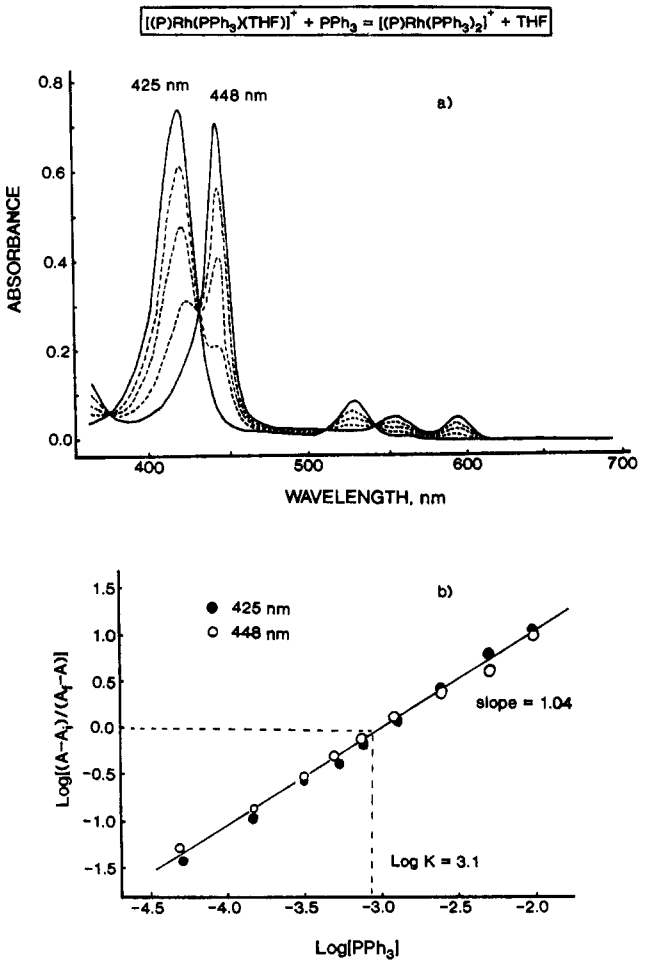

Figure 2. (a) UV–visible spectral changes obtained upon addition of PPh_3 to $[(P)Rh(PPh_3)_2]^+$ in THF and (b) analysis of spectral data at 425 (●) and 448 nm (○).

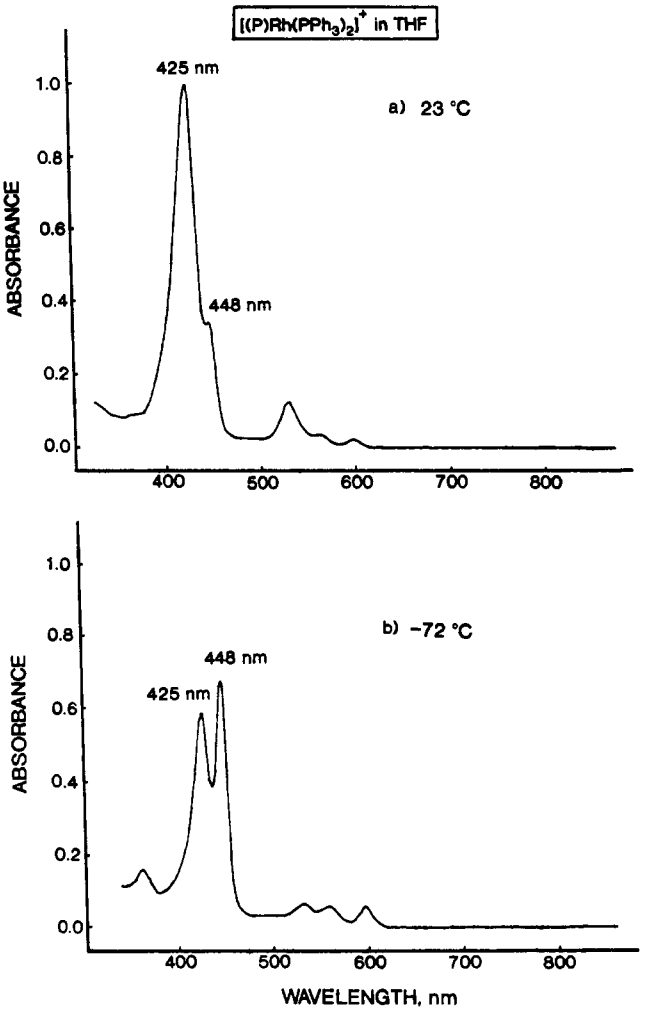

Figure 3. UV–visible spectra of $[(P)Rh(PPh_3)_2]^+$ in THF and 0.2 M $TBAPF_6$ at (a) 23 °C and (b) –72 °C.

A conversion of $[(P)Rh(PPh_3)(THF)]^+$ back to the original $[(P)Rh(PPh_3)_2]^+$ species could also be accomplished by simply lowering the solution temperature from 23 to –72 °C, and the resulting UV–visible spectra at these two temperature extremes are shown in Figure 3. As seen in this figure, the 425- and 532-nm bands of $[(P)Rh(PPh_3)(THF)]^+$ are decreased in intensity at –72 °C, and under these conditions, the characteristic bands of $[(P)Rh(PPh_3)_2]^+$ at 448, 557, and 597 nm are well-defined. These results indicate that formation of the bis-PPh_3 complex is favored in THF at low temperature and that an approximate 50:50 mixture of $[(P)Rh(PPh_3)(THF)]^+$ and $[(P)Rh(PPh_3)_2]^+$ is present in THF at –72 °C.

Reduction of $[(P)Rh(PPh_3)_2]^+$. Cyclic voltammograms of $[(P)Rh(PPh_3)_2]^+$ at 23 and –72 °C are shown in Figure 4. The first reduction involves an irreversible addition of one electron at room temperature, and this process (peak 1) is characterized by a peak at E_p = –0.58 V for a scan rate of 100 mV/s. The second reduction (peak 3) is reversible and is located at $E_{1/2}$ = –1.81 V. An irreversible reoxidation process (peak 4) also appears at E_p = –0.25 V for a scan rate of 100 mV/s.

The first reduction of $[(P)Rh(PPh_3)_2]^+$ remains irreversible at –72 °C (see Figure 4b), and under these conditions, processes 1 and 3 are negatively shifted to E_p = –0.85 V and $E_{1/2}$ = –1.92 V for a scan rate of 100 mV/s. An additional irreversible reduction is also present at E_p = –1.20 V and only appears at low temperature. This process was not further investigated in the present study, but its occurrence may be related to the fact that two different species, $[(P)Rh(PPh_3)(THF)]^+$ and $[(P)Rh(PPh_3)_2]^+$, are detected in the UV–visible spectrum of this solution at low temperature (see Figure 3).

The irreversible anodic peak 4, as well as the reversible peak 3, are similar to processes reported in the literature for the reduction and oxidation of $[(P)Rh^{II}]_2$ in THF,[4-6] and this suggests that the same bimetallic Rh(II) dimer is also generated in the present study after the first reduction of $[(P)Rh(PPh_3)_2]^+$. The thin-layer UV–visible spectra of the electroreduction products have bands at ~406 and 497 nm (see Table I and Figure 4) and are in agreement with this assignment.

Reduction of $[(P)Rh(PPhMe_2)_2]^+$. Cyclic voltammograms of $[(P)Rh(PPhMe_2)_2]^+$ at 23 and –72 °C are shown in Figure 5. Two reversible reductions are observed at all temperatures and scan rates. The first occurs at $E_{1/2}$ = –0.97 V (23 °C) or –1.03 V (–72 °C) while the second is located at $E_{1/2}$ = –1.70 V and does not vary significantly with temperature. A small prepeak also appears at E_p = –0.95 V and may be due to an unknown minor impurity.

Thin-layer UV–visible spectra obtained after reduction of $[(P)Rh(PPhMe_2)_2]^+$ at two different temperatures are shown in Figures 5a and 5b. These spectra change little with temperature and are characterized by a Soret band at 467–468 nm and two weak, broad bands at 720–722 and 886–890 nm (see Table I). They are also similar to the spectrum reported for reduced $[(P)Rh(PPhMe_2)_2]^+$ in CH_2Cl_2.[9]

Reduction of $[(P)Rh(PPh_2Me)_2]^+$. Temperature-dependent cyclic voltammograms of $[(P)Rh(PPh_2Me)_2]^+$ and the related UV–visible spectra of the reduction products at two different temperatures are shown in Figure 6. The room temperature voltammogram has characteristics of both $[(P)Rh(PPh_3)_2]^+$ and $[(P)Rh(PPhMe_2)_2]^+$, but this is not the case at –72 °C, where two reversible processes are observed.

Table I. Half-Wave Potentials ($E_{1/2}$) and Spectral Peak Maxima (λ, nm) before and after Electroreduction of Rhodium Porphyrins in THF Containing 0.2 M $TBAPF_6$

temp, °C	compound	$E_{1/2}$, V vs SCE	λ_{max}, nm: before reduction			after reduction[c]		
23	$[(P)Rh(PPh_3)_2]^+$ [a]	−0.58[b]	425	532		405	497	
	$[(P)Rh(PPh_2Me)_2]^+$	−0.85[b]	446	557	595	405	498	
	$[(P)Rh(PPhMe_2)_2]^+$	−0.97	445	557	596	467	722	886
−72	$[(P)Rh(PPh_3)_2]^+$	−0.85[b]	448	557	597	407	497	
	$[(P)Rh(PPh_2Me)_2]^+$	−1.04	446	557	595	466	722	880
	$[(P)Rh(PPhMe_2)_2]^+$	−1.06	445	557	596	468	720	890

[a] Initial species in solution at room temperature is identified as $[(P)Rh(PPh_3)(THF)]^+$ (see text). [b] Irreversible reduction. Value listed is E_p obtained at a scan rate of 100 mV/s. [c] Spectra obtained after controlled-potential reduction by one electron.

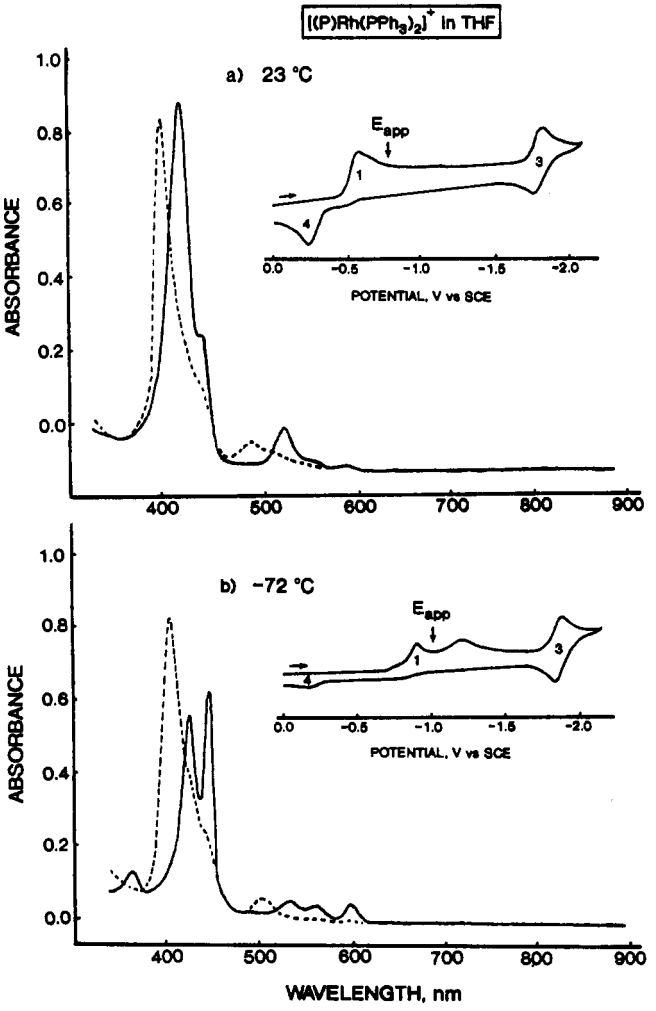

Figure 4. Thin-layer UV–visible spectra obtained before (—) and after (···) controlled-potential reduction of $[(P)Rh(PPh_3)_2]^+$ in THF containing 0.2 M $TBAPF_6$ at (a) 23 °C and (b) −72 °C. The figure insets show cyclic voltammograms obtained at the same temperatures in THF containing 0.1 M $TBAPF_6$.

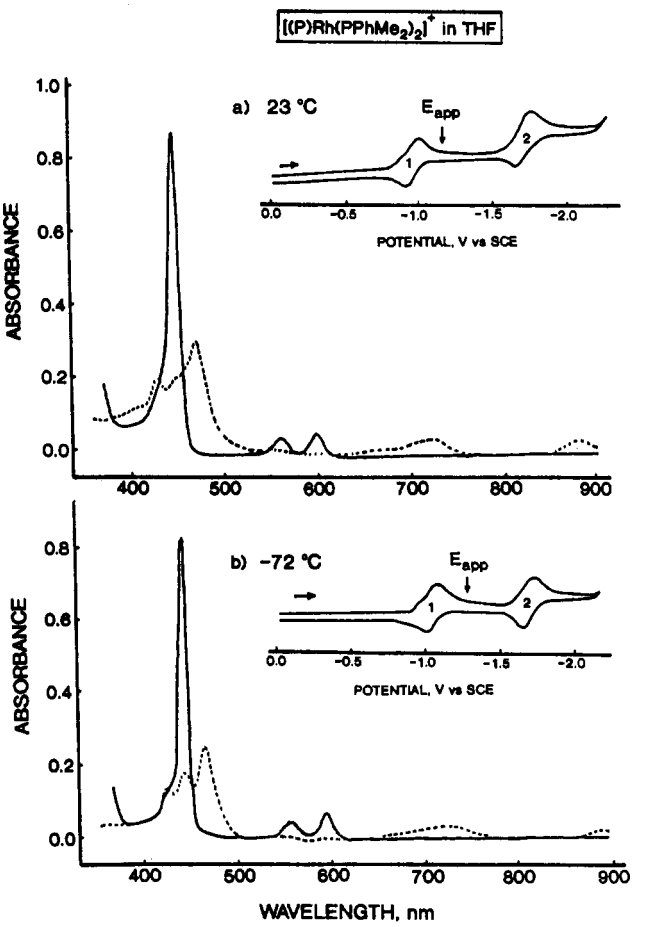

Figure 5. Thin-layer UV–visible spectra obtained before (—) and after (···) controlled-potential reduction of $[(P)Rh(PPhMe_2)_2]^+$ in THF containing 0.2 M $TBAPF_6$ at (a) 23 °C and (b) −72 °C. The figure insets show cyclic voltammograms obtained at the same temperatures in THF containing 0.1 M $TBAPF_6$.

The spectral changes obtained during reduction of $[(P)Rh(PPh_2Me)_2]^+$ at room and low temperature are shown in Figure 6b. The spectrum of the reduced species at room temperature has bands at 405 and 498 nm and can be characterized as $[(P)Rh]_2$. In contrast, the product of the one-electron reduction at low temperature can be assigned as a porphyrin π anion radical. This UV–visible spectrum has bands at 466, 722, and 880 nm and is almost identical to the spectrum obtained after a controlled-potential one-electron reduction of $[(P)Rh(PPhMe_2)_2]^+$ in THF (see Table I and Figure 5).

Reduction of $(P)Rh(PF_3)(OH)$. Cyclic voltammograms of $(P)Rh(PF_3)(OH)$ at 23 and −72 °C are shown in Figures 7a and 7b, respectively. Three reductions are observed at both room and low temperature. The first room temperature reduction occurs at $E_{1/2} = -1.24$ V and is reversible when the potential scan is reversed prior to the addition of a second electron, at which point it becomes irreversible. The second reduction (peak 2 in Figure 7a) is not coupled to a reoxidation process and is characterized by an $|E_p - E_{p/2}| = 60 \pm 5$ mV, suggesting a one-electron transfer followed by an irreversible chemical reaction. A third reversible reduction is located at $E_{1/2} = -1.84$ V and is associated with the chemically generated product formed after the second one-electron transfer. The product formed after the second reduction can also be reoxidized, and this reaction (labeled peak 4) is located at $E_p = -0.22$ V for a scan rate of 0.1 V/s. This oxidation peak is at a potential associated with the irreversible oxidation of electrogenerated $[(P)Rh]_2$[7,8] and is not observed if the initial negative scan is terminated at potentials positive of the second reduction. The overall reduction behavior of $(P)Rh(PF_3)(OH)$ is similar to that of $[(P)Rh(PPh_2Me)_2]^+$ in THF at −10 °C (see Figure 6).

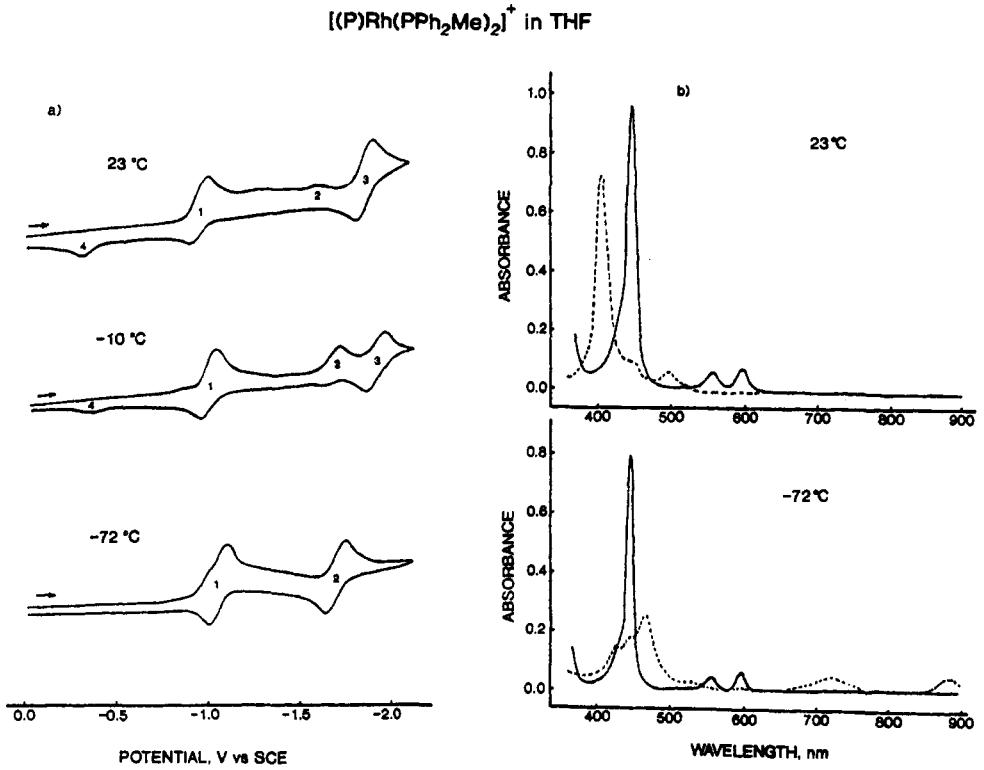

Figure 6. (a) Temperature-dependent cyclic voltammograms of $[(P)Rh(PPh_2Me)_2]^+$ in THF and 0.1 M $TBAPF_6$ and (b) thin-layer UV–visible spectra obtained before (—) and after (···) controlled-potential reduction of $[(P)Ph(PPh_2Me)_2]^+$ at the 23 and −72 °C.

Table II. Half-Wave Potentials ($E_{1/2}$) for Oxidation and Reduction of Rh(III) Complexes

axial ligand		RT oxidation[a]			LT reduction[b]		
fifth	sixth	first	second	ΔE, V	first	$\lvert E_{ox} - E_{re}\rvert$[f]	ref
PPh_3	PPh_3	1.22	1.64[c]	0.42	−0.85[e]		tw
PPh_2Me	PPh_2Me	1.18	1.70	0.52	−1.04	2.22	tw
$PPhMe_2$	$PPhMe_2$	1.19	1.72	0.53	−1.06	2.25	tw
PF_3	OH^-	1.05	1.48	0.43	−1.24	2.29	tw
$CNCH_2Ph$	$CNCH_2Ph$	1.14	1.47	0.33	−0.98	2.12	tw
$:C(NHCH_2Ph)_2$		1.27	1.49	0.22	−1.01	2.28	tw
$NHMe_2$	$NHMe_2$	1.27[d]	1.70[d]	0.43[d]	−1.05	2.32	8
$NHMe_2$	Cl^-	1.00[d]	1.43[d]	0.43[d]	−1.31[e]		8
C_2H_5		0.97[d]	1.35[d]	0.38[d]	−1.41	2.38	6
Cl^-		0.98	1.36	0.38			3
NO		0.94	1.36	0.42			3

[a] Reversible oxidations measured at room temperature in CH_2Cl_2 containing 0.1 M $TBAPF_6$ unless otherwise indicated. [b] Reversible reductions measured at −72 °C in THF containing 0.1 M $TBAPF_6$ unless otherwise indicated. [c] Another reversible peak is observed at $E_{1/2}$ = 1.77 V. [d] Potentials obtained in PhCN containing 0.1 M $TBAPF_6$. [e] Irreversible reduction. Value listed is E_p obtained at a scan rate of 100 mV/s. [f] Absolute potential difference between first reversible oxidation in CH_2Cl_2 and first reversible reduction in THF. tw = this work.

The UV–visible spectrum of $(P)Rh(PF_3)(OH)$ before electroreduction is characterized by a Soret band at 420 nm and a single Q band at 527 nm. Both bands decrease in intensity after the controlled potential addition of one electron at −1.50 V. The first electroreduction product has a Soret band at 445 nm and two weak broad bands at 653 and 890 nm (see Figure 8, top). The spectrum obtained during the first 30 s of electrolysis is similar to the one obtained after a one-electron reduction of $[(P)Rh(PPhMe_2)_2]^+$ and is assigned as a Rh(III) porphyrin π anion radical. This spectrum is not constant with time but continues to change, as illustrated in Figure 8, bottom. The spectrum obtained after 180 s has bands at 405 and 495 nm and has previously been assigned to $[(TPP)Rh]_2$. This final spectrum can be converted to the initial spectrum of $(P)Rh(PF_3)(OH)$ when a positive potential is reapplied.

Reduction of $[(P)Rh{=}C(NHCH_2Ph)_2]^+$ and $[(P)Rh(CNCH_2Ph)_2]^+$. Cyclic voltammograms of $[(P)Rh{=}C(NHCH_2Ph)_2]^+$ and $[(P)Rh(CNCH_2Ph)_2]^+$ at room and low temperature are shown in Figure 7, which also illustrates the cyclic voltammograms of $(TPP)Rh(PF_3)(OH)$. UV–visible spectra obtained at low temperature during the first one-electron reduction of $[(P)Rh{=}C(NHCH_2Ph)_2]^+$ and $[(P)Rh(CNCH_2Ph)_2]^+$ are similar to spectra obtained after a one-electron reduction of $[(P)Rh(PPhMe_2)_2]^+$ in THF. The spectra are also similar to the spectrum of electroreduced $(P)Rh(PF_3)(OH)$ (see Table III) and are all characteristic of a porphyrin π anion radical.

Oxidation of Complexes. A summary of half-wave potentials for oxidation of the six investigated compounds is given in Table II. Each porphyrin undergoes two diffusion-controlled one-electron oxidations, and this is also the case for other previously investigated Rh(III) porphyrins.[3,6,8] The absolute potential difference between the two oxidations of each complex containing a phosphine, carbene, or isocyanide axial ligand ranges between 0.22 and 0.53 V, and these values can be compared with an average separation of 0.40 ± 0.03 V for Rh(III) porphyrins containing an amine, chloride, nitric oxide, or a σ-bonded axial ligand (see Table II).

Overall Mechanism. The cyclic voltammetric and UV–visible spectroelectrochemical data are self-consistent and indicate that one of two possible products are formed after addition of one electron to the investigated Rh(III) porphyrins. One of these is assigned as a Rh(III) π anion radical while the other is assigned

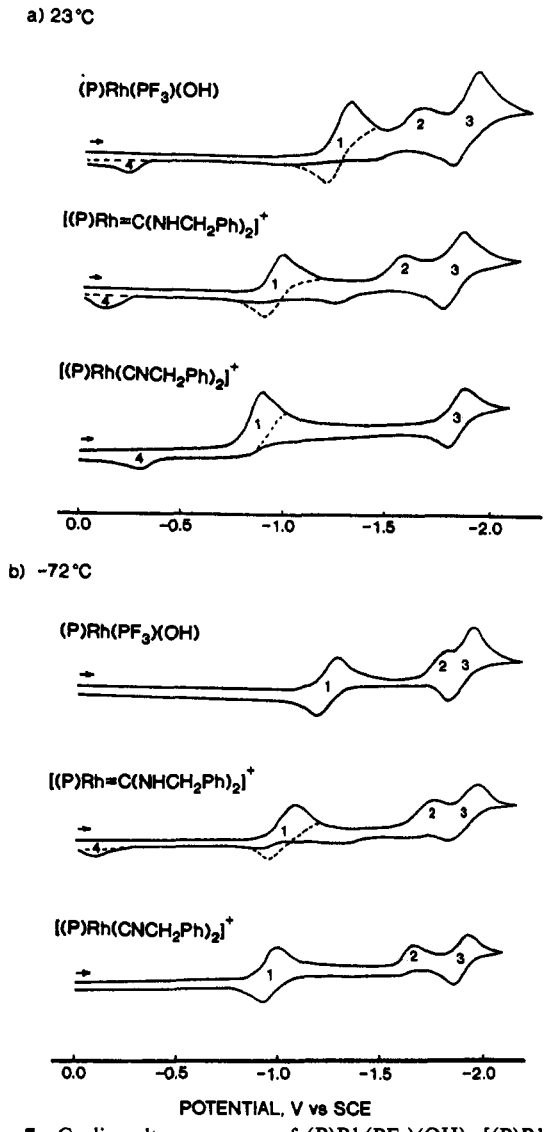

Figure 7. Cyclic voltammograms of (P)Rh(PF_3)(OH), [(P)Rh=C($NHCH_2Ph$)$_2$]$^+$, and [(P)Rh($CNCH_2Ph$)$_2$]$^+$ in THF containing 0.1 M $TBAPF_6$ at (a) 23 °C and (b) −72 °C.

as dimeric [(P)Rh]$_2$ which has bands at 405 and 497 nm. The UV–visible data show only the final electroreduction product on the spectroelectrochemical time scale and give no indication about the site of electron transfer prior to formation of the dimer. However, a similar mechanism is proposed to occur for reduction of all six investigated Rh(III) complexes in THF, and a suggested sequence of steps leading from the initial five- or six-coordinated complex to a Rh(III) porphyrin π anion radical or a Rh(II) dimer is given in Figure 9.

Relatively stable porphyrin π anion radicals are obtained at low temperature after the first one-electron reduction of [(P)Rh(PPh_2Me)$_2$]$^+$, [(P)Rh($PPhMe_2$)$_2$]$^+$, [(P)Rh=C($NHCH_2Ph$)$_2$]$^+$, or [(P)Rh($CNCH_2Ph$)$_2$]$^+$ (see Figures 5 and 6 and Table III), but only dimeric [(P)Rh]$_2$ is observed during reduction of [(P)Rh(PPh_3)$_2$]$^+$ where no π anion radical intermediate can be detected (see Figure 4). (P)Rh(PF_3)(OH) has behavior intermediate between the above two extremes. The spectroelectrochemical data is given in Figure 8 and clearly illustrates the conversion between an initial porphyrin π anion radical spectrum and that of dimeric [(P)Rh]$_2$ over a period of 30–180 s after initiation of electrolysis.

Additional indirect evidence for the initial formation of a porphyrin π anion radical comes from an internal comparison of half-wave potentials for oxidation and reduction of the different Rh(III) complexes as well as from a comparison of data for these

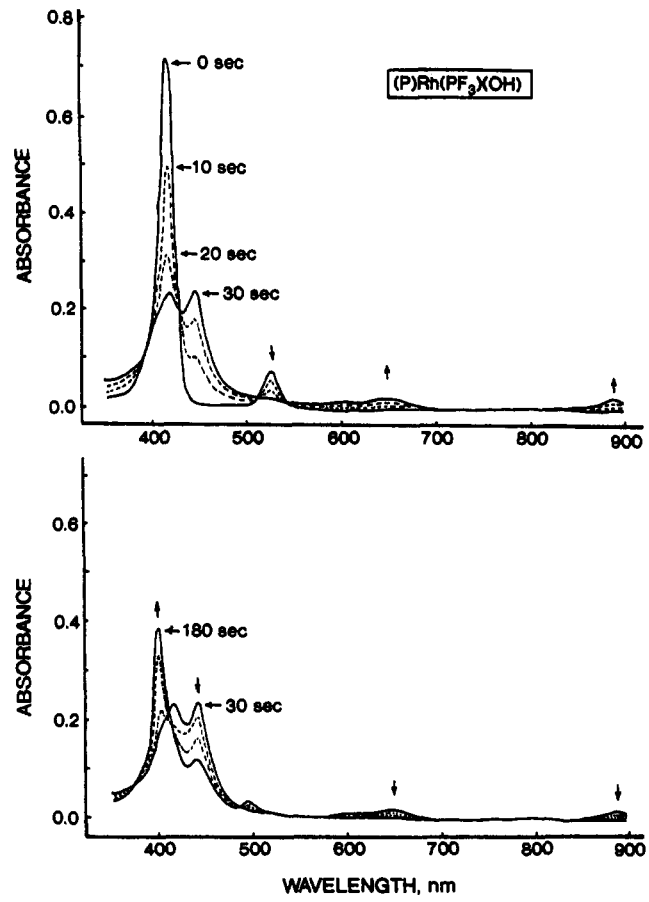

Figure 8. Time-resolved UV–visible spectra obtained during controlled-potential reduction of (P)Rh(PF_3)(OH) at −1.50 V in THF containing 0.2 M TBAP (top) from 0 to 30 s and (bottom) from 30 to 180 s.

Table III. Spectral Peak Maxima (λ, nm) before and after Electroreduction of Rhodium Porphyrins in THF Containing 0.2 M $TBAPF_6$

compound	$E_{1/2}$, V vs SCE	λ_{max}, nm[a] before reduction			after reduction		
(P)Rh(PF_3)(OH)	−1.24	420	527		445	653	890
[(P)Rh($CNCH_2Ph$)$_2$]$^+$	−0.98	425	539		453	680	885
[(P)Rh=C($NHCH_2Ph$)$_2$]$^+$	−1.01	422	533		442	648	880

[a] Values given for solutions at −72 °C.

species to that for other porphyrin complexes where all of the electrode reactions involve only the conjugated π ring system. Unfortunately, reversible potentials for both oxidation and reduction of the same Rh complex could not be measured in a single given solvent, but $E_{1/2}$ values for the reversible room temperature oxidation in CH_2Cl_2 and the low-temperature reduction in THF could still be obtained, and these values give an approximate HOMO–LUMO gap for each investigated compound.

Five of the six investigated compounds are reversibly reduced between $E_{1/2}$ = −0.98 and −1.24 V at low temperature (the bis-phosphine derivative reduction is irreversible) (see Table II) while the first reversible oxidation of the same compounds occurs between $E_{1/2}$ = +1.05 and +1.27 V at room temperature. The absolute potential difference between these room temperature oxidations and the low-temperature reductions (where no chemical reactions occur) averages 2.23 V and ranges between a low of 2.12 V for [(P)Rh($CNCH_2Ph$)$_2$]$^+$ and a high of 2.29 V for (P)-Rh(PF_3)(OH). The average separation of 2.23 V fits well the experimentally measured difference of 2.25 ± 0.15 V which is observed when both electrode reactions involve the porphyrin π

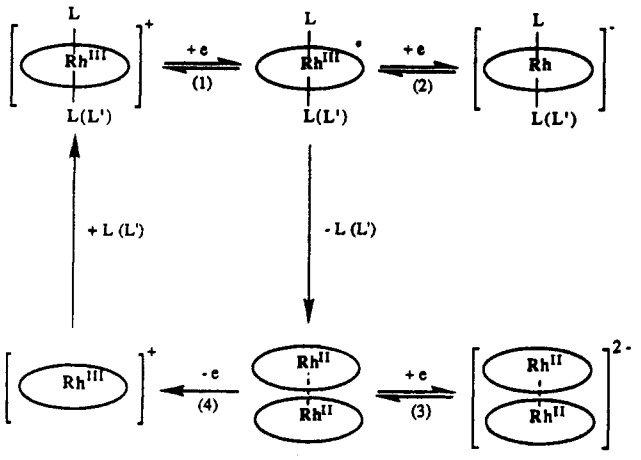

Figure 9. Proposed electron-transfer scheme for reduction of $[(TPP)Rh(L)_2]^+$ complexes in THF. The specific electron-transfer steps 1–4 correspond to peaks given in Figures 5–7.

ring system.[15] It is also only slightly lower than the separation of 2.32–2.38 V for the oxidation and reduction of $[(P)Rh(NHMe_2)_2]^+$ or $(P)Rh(C_2H_5)$ under similar solution conditions (see Table II). The site of reduction in the case of the latter σ-bonded compound is clearly at the porphyrin π ring system,[10] and this now also appears to be the case for all Rh(III) porphyrins which have to date been electrochemically investigated.

It is also worth pointing out that $E_{1/2}$ for reduction of the positively-charged complexes (those in which the anionic axial ligand is dissociated) spans only a range of 0.08 V at low temperature ($E_{1/2}$ varies from 0.98 to 1.06 V) independent of the axial ligand. This further suggests that the first one-electron addition to these Rh(III) porphyrins does not give a Rh(II) complex but rather a π anion radical since a reduction at the metal center should be accompanied by a much larger substituent effect of the axial ligand as was observed for the reduction of iron(III) and cobalt(III) tetraphenylporphyrins under similar solution conditions.[15] Also, it should be noted that the first one-electron reduction of both $(P)Rh(PF_3)(OH)$ and $(P)Rh(NHMe_2)Cl$ occurs at more negative potentials than for reduction of the singly-charged derivatives (see Table II), and this can be simply accounted for by the lack of a positive charge on the six-coordinate complexes which have an associated rather than dissociated counteranion.

Acknowledgment. The support of the National Science Foundation (Grant CHE 8822881), the National Institutes of Health (Grant 25172), and an LGIA grant from the University of Houston is gratefully acknowledged.

(15) Kadish, K. M. *Prog. Inorg. Chem.* **1986**, *34*, 435.